Characterization of UHF PD Sensors for Power Transformers Using an Oil-filled GTEM Cell

Martin Siegel, Michael Beltle and **Stefan Tenbohlen**
University of Stuttgart
Institute of Power Transmission and High Voltage Technology (IEH)
Pfaffenwaldring 47
70569 Stuttgart, Germany

ABSTRACT

Common reasons for local failures in power transformers are partial discharges (PD) in the electric insulation. The ultra-high frequency (UHF) PD measurement method gained in importance for transformer diagnosis and monitoring within the last years. Due to its robustness against external noise, it is suitable for both, factory acceptance tests (FAT) and site acceptance tests (SAT). For the application at acceptance tests, it is necessary that the UHF technique is a reliable testing method and also comparable between different UHF measurement systems. Therefore, the UHF sensor's characteristic has to be included in a calibration procedure by using its antenna factor (AF). This contribution implements a custom-built oil-filled Gigahertz-Transversal-Electromagnetic cell (GTEM cell) for the AF evaluation. In the first part, the GTEM cell's design and dimensioning are illustrated and the cell is evaluated in terms of its high frequency behavior. The second part determines the AF of two different UHF sensor types: UHF Drain Valve Sensors and UHF Plate Sensors using the GTEM cell. Additionally, the influences of insertion depths and standardized gate valves on the Drain Valve Sensor's AF are taken into account.

Index Terms - **Power transformers, Partial discharges, UHF measurements, UHF antennas, Calibration.**

1 INTRODUCTION

POWER transformers can be considered as an essential part to assure the reliability of the electrical grid. Transformer failures lead to consequential damage with accordant costs. Reliable operation of power transformers is fundamental for service security. Damages in the insulation of a power transformer, like local defects, must ideally be recognized at an early stage. Different diagnostic methods have been established to meet the deriving demands for onsite and factory measurements. Electrical PD measurement found its way into standard testing according to IEC 60270 [1]. Within the last decades, alternative measurement methods for PD arose. Originally used within gas insulated switchgears (GIS) [2], ultra-high frequency (UHF: 300 MHz – 3 GHz) PD measurement is nowadays also adapted for power transformers' diagnosis [3, 4]. UHF has been established as a trigger for acoustic PD localization [3], for onsite/online diagnostic PD measurements [6] and seems also to be suitable for online PD monitoring [7]. UHF measurements are electromagnetically shielded against external disturbances, e.g. corona, by the grounded transformer tank. Hence, UHF is often advantageous in onsite PD measurements, as Figure 1 illustrates. This makes it suitable for a variety of different applications, e.g. comparison of offsite measurement at FAT with online, onsite measurements (after transportation and installation at SAT).

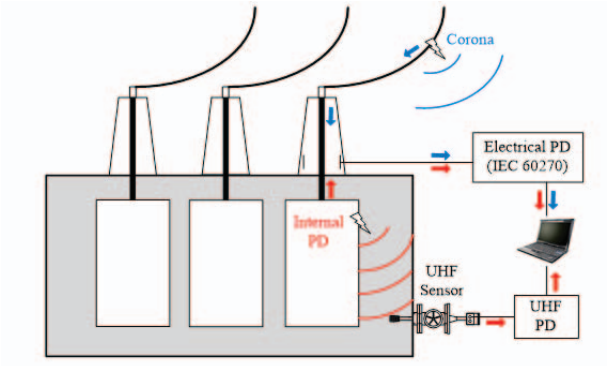

Figure 1. Power Transformer with electrical and UHF PD measurement [8]. Corona signals are attenuated by the bushing capacity and are not measured by the UHF sensor but superimpose the electrical measurement.

Both, electrical and UHF PD levels, are influenced by the

- type and real level of the PD source
- signal attenuation in the particular coupling path
- sensor sensitivity
- sensitivity of the measurement device

Manuscript received on 31 July 2015, in final form 8 February 2016, accepted 22 February 2016.

DOI: 10.1109/TDEI.2016.005562

The influence of the measurement equipment (coupling capacity, quadrupole and the measurement recorder) can be compensated by using calibration for the electric measurement (as described in IEC 60270). It is a fact that the actual PD level cannot be estimated due to the unknown signal path attenuation and unknown internal capacitances [9, 10]. Nevertheless, calibration enables the apparent charge as an acceptance level within transformer routine tests as a result of the comparability between different measurement systems.

The UHF method can also provide calibration but the procedure differs from its electrical pendant in one aspect. The transfer function (TF) of the coupling device (coupling capacitor and quadrupole) can be included into the calibrated path of the electrical measurement by injecting a calibration signal between transformer and coupling capacitor, see Figure 2, upper plot. The coupling device for the UHF method is represented by the UHF sensor, which is inserted into the transformer. Hence, a similar injection of a calibration signal is not possible. Nevertheless, calibration using a standardized signal can be used for the remaining signal path (cable and PD recorder), see Figure 2, lower plot. This calibration is considered insufficient because the sensor's TF cannot be neglected in general. The sensor can be included into the calibrated path if its TF has previously been measured. One possibility to determine the TF is the antenna factor (AF) measurement.

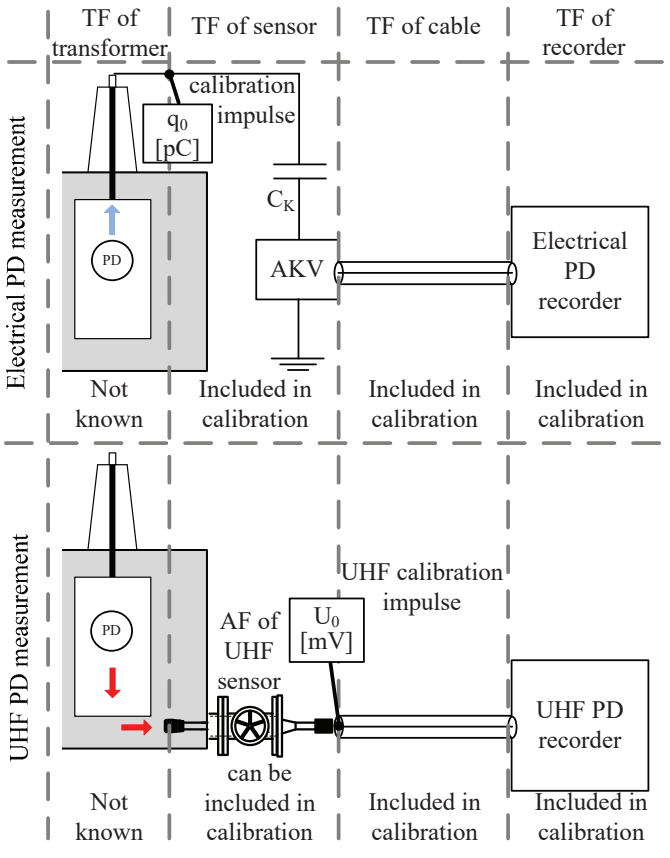

Figure 2. Comparison of PD calibration methods.
Upper plot: calibration of electrical measurement.
Lower plot: calibration proposal for UHF measurement.

The AF of UHF sensors already has been determined within an air-filled TEM cell in a frequency range up to 950 MHz in previous investigations [11]. Conventional TEM cells suffer from two drawbacks: The full bandwidth of UHF sensors cannot be tested due to the cells' frequency limits $f < 1$ GHz.

Additionally, the AF measured in air is not applicable in transformer oil because of different relative permittivities and needs to be shifted in frequency range [11, 12]. Hence, AF measurements at inside-transformer conditions and at full UHF frequency range are preferable. To meet these conditions, an oil-filled Gigahertz Transverse Electromagnetic (GTEM) cell is required, see Figure 4 [13].

2 UHF SENSOR CHARACTERIZATION

The antenna sensitivity depends on its design in relation to the electromagnetic wavelength. Antennas are described by different characteristics, e.g. by the antenna gain or the antenna aperture. The antenna gain of non-flat top antennas like monopoles or dipoles is often specified by the effective length l_{eff} [12] or the antenna factor AF, which is defined for a receiving antenna as

$$AF(f) = \frac{E(f)}{U(f)} \tag{1}$$

where $U(f)$ is the voltage at the antenna terminal and $E(f)$ is the electric field strength at the antenna [14]. The effective length is defined by the inverse AF. The higher the antenna's sensitivity, the smaller is the antenna factor. The antenna sensitivity evaluation requires a special setup which provides a defined homogeneous electric field without external disturbances and without internal reflections of electromagnetic waves.

2.1 TEM CELL TYPES

These requirements are met by a special equipped EMC absorber room or a GTEM cell, which simulates a free space planar wave for susceptibility testing purposes concerning electromagnetic compatibility [13]. A solely vertically orientated, homogeneous electromagnetic field can be applied to the equipment under test (EUT) in the testing volume of the GTEM cell without interference from the ambient electromagnetic environment. The GTEM cell geometry is a constantly expanding transmission line without a second taper or output terminal at its end, see Figure 3. The inner conductor is terminated in the cell with its wave impedance to avoid reflections. Electromagnetic (EM) absorbers are used as termination for planar waves.

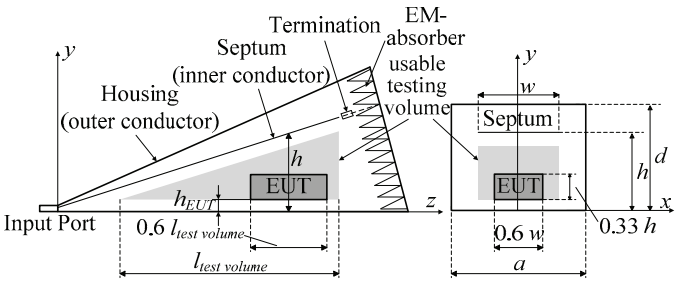

Figure 3. Schematic of GTEM cell. Side view (left) and cross section (right).

Ideally, the termination should provide a reflection factor $r_{termination} = 0$. Rectangular transmission line geometry is used over the whole cell length. The septum is positioned eccentric to

provide a testing volume of sufficient size for the EUT. Typically, the ratio between septum height *h* and cell height *d* is kept constant at values between 2/3 and 3/4 throughout the cell.

2.2 PRINCIPLE OF MEASUREMENT

The electrical field in the cell is generated by a defined power signal at Port 1 using a vector network analyzer (VNA). The resulting voltage at the UHF sensor is measured at Port 2 using scattering parameters. The UHF sensor antenna is positioned in the test volume of the cell. The AF can be calculated according to equation (1) with known homogenous field conditions of the cell and the antenna voltage from the measurement.

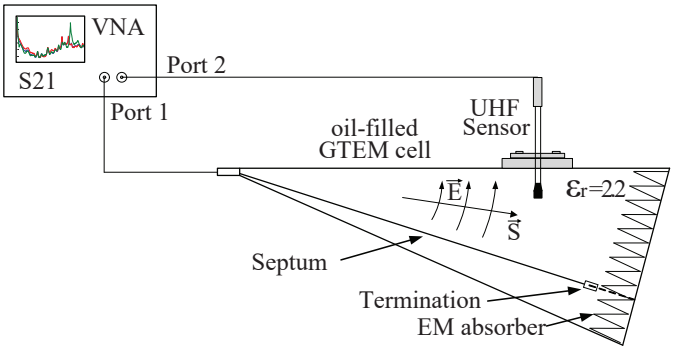

Figure 4. Schematic of test setup for UHF antennas using an oil-filled GTEM cell.

3 CELL DESIGN

The volume is chosen to be as large as possible in order to meet homogenous field requirements for small and large antenna designs. Therefore, the *h/d*-ratio is chosen as 3/4 in order to increase volume height. The remaining degree of freedom given by the *w/a*-ratio is used to adjust the cell's wave impedance.

3.1 WAVE IMPEDANCE

The entire cell's wave impedance has to be $Z = 50\ \Omega$ in order to avoid reflections at the input and the termination. *Z* is defined by the per-unit-length parameters given by the equivalent circuit of an infinitesimal short line element: The series inductance *L'*, the series resistance *R'*, the parallel conductance *G',* and the parallel capacity *C'*, see equation (2) [15].

$$Z = \sqrt{\frac{R' + j\omega L'}{G' + j\omega C'}} \tag{2}$$

In this setup, both ohmic components *R'* and *G'* can be neglected because of the low electrical resistivity of the septum material (copper) and the low conductivity of the oil in the cell. This leads to the simplified equation (3) for *Z*.

$$Z = \sqrt{\frac{L'}{C'}} \tag{3}$$

L' and *C'* have to be estimated for every per-unit-length parameter of the GTEM cell. Both are defined by the line element's cross section geometry. All parameters are shown in Figure 5, where *d* represents the height of the cross section; *h* is the height of the septum in the cell; *u* is the septum's thickness and *w* its width. The septum thickness *u* becomes negligible if it is small compared to the cell height *d*. The simplification is valid for the major part of the cell but not for the inlet of the cell, called apex. Therefore, the apex is considered separately.

The cell's wave impedance *Z* can be determined using analytic approximating methods or numeric simulations, e.g. field solving algorithms like the finite element method (FEM).

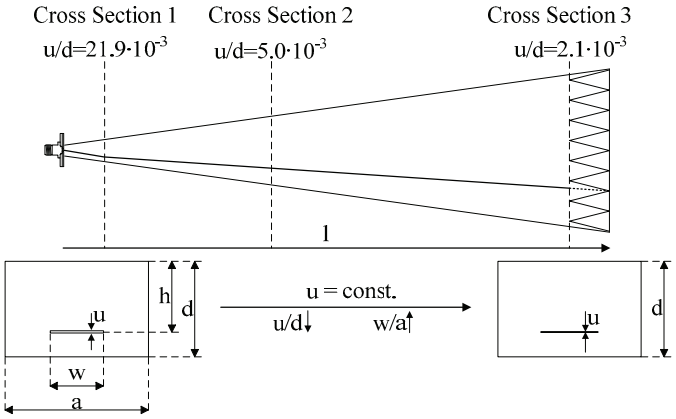

Figure 5. *u/d* and *w/a*-ratios along the GTEM cell length at different cross sections [16].

3.2 ANALYTICAL APPROXIMATION

The first approach uses an approximation method which estimates the capacitance of a rectangular coaxial transmission line with an infinitely thin and vertically eccentric septum; also see [17]. As the inner conductor thickness ($u = 0$) is neglected in this method, it is not suitable for the apex impedance calculation. The apex is designed using a numerical approach, see chapter 3.4.

The capacitance can be calculated using equation (4) were *K*, V_{1n}, V_{2n} and g_n are substitutes defined in equations (5) to (8) [17].

$$C = \frac{2\varepsilon_0\left(1 + \frac{K}{4}\right)^2}{a\sum_{n=1}^{\infty}\left(\frac{1}{w}[V_{1n} + KV_{2n}]\right)^2 g_n} \tag{4}$$

$$K = -\frac{\sum_{n=1}^{\infty}(4V_{2n} - V_{1n})V_{1n}g_n}{\sum_{n=1}^{\infty}(4V_{2n} - V_{1n})V_{2n}g_n} \tag{5}$$

$$V_{1n} = \frac{4}{n\pi}\sin\left(\frac{n\pi}{2}\right)\sin\left(\frac{n\pi w}{2a}\right) \tag{6}$$

$$V_{2n} = \frac{2w}{a}\sin\left(\frac{n\pi}{2}\right)\left(\frac{\sin\left(\frac{n\pi w}{2a}\right)}{\left(\frac{n\pi w}{2a}\right)} + \frac{3}{\left(\frac{n\pi w}{2a}\right)^2}\left[\cos\left(\frac{n\pi w}{2a}\right) - \frac{2\sin\left(\frac{n\pi w}{2a}\right)}{\left(\frac{n\pi w}{2a}\right)} + \frac{\sin\left(\frac{n\pi w}{4a}\right)^2}{\left(\frac{n\pi w}{4a}\right)^2}\right]\right) \tag{7}$$

$$g_n = \frac{a}{\varepsilon_r n\pi\left(\coth\left[\frac{n\pi h}{a}\right] + \coth\left[\frac{n\pi(d-h)}{a}\right]\right)} \tag{8}$$

The speed of light in a medium equals the phase velocity v_{phase} of the lossless transmission line, which is defined by the

angular frequency ω and the according phase coefficient $\beta_{lossless}$, see equation (9).

$$c_{medium} = v_{phase} = \frac{\omega}{\beta} \quad , \quad \beta_{lossless} = \omega\sqrt{L'C'} \tag{9}$$

The characteristic impedance Z can be calculated using the provided capacity C' of the line segment. Z can be defined by either using the speed of light c_{medium} in the oil-filled cell or by the speed of light in vacuum c_{vacuum} and typical oil permeability $\varepsilon_{r,oil} = 2.2$ (equation (10)). The oil is assumed to be a non-dispersive medium for all following considerations with constant permeability. Hence, group velocity and phase velocity are the same [18].

$$Z = \frac{1}{c_{medium}C} = \frac{\sqrt{\varepsilon_r}}{c_{vacuum}C} \tag{10}$$

Figure 6 shows the calculated impedance Z depending on the *w/a*-ratio at three different *h/d*-ratios. The line impedance can be kept constant at any chosen cross section if the geometric properties of the cross section remain constant. In order to keep the *h/d*-ratio = 3/4 constant, the septum has to be designed to meet a *w/a*-ratio of approx. *w/a* = 2/5.

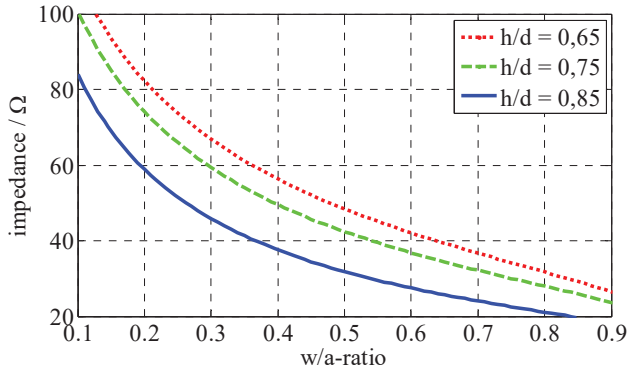

Figure 6. Line impedance Z of the oil-filled GTEM cell depending on its *w/a*-ratio and its *h/d*-ratio [8].

3.3 NUMERICAL MODEL

The results of the analytical model are checked by a numerical model. A FEM field solver is used to calculate the wave impedance of the cell. It is sufficient to perform a 2D simulation for the electric and magnetic field distribution of the cross sections as the cross sections and hence the cell's wave impedance are independent of the cell length. The capacitance C' and inductance L' can be calculated by equations (11) and (12) using the magnetic field energy delivered by the field solver.

$$W'_{el.} = {}^1\!/_2 \; C' \hat{u}^2 \tag{11}$$

$$W'_{magn.} = {}^1\!/_2 \; L' \hat{\imath}^2 \tag{12}$$

The wave impedance is calculated from C' and L' according equation (3). Figure 7 illustrates the simulated dependency between wave impedance and *w/a*-ratio at three different cross sections (see Figure 5) which only differ in their *u/d*-ratio. The influence of the septum's thickness u is a parallel translation of the impedance curve with decreasing impedances at increasing *u/d*-ratios. The numerical solution and the analytical approach can be compared at cross sections with small *u/d*-ratio (cross sections 2 and 3). The simulation at cross sections 2 matches the analytic result exactly; cross section 3 shows little deviation.

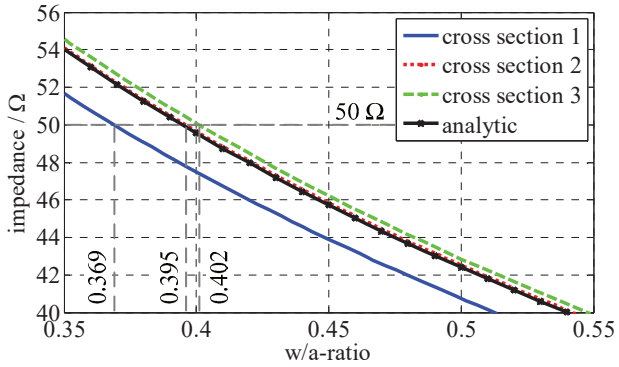

Figure 7. Calculated wave impedance Z for cross sections depending on the *w/a* ratio.

3.4 SEPTUM GEOMETRY

The numerical model is used for cell dimensioning, because the FEM includes the septum thickness u. Again, the *w/a*-ratio is the remaining variable which is optimized along the cell in order to keep the *h/d*-ratio = 3/4 constant. Exemplary, the three cross sections from Figure 5 are used to estimate the cell geometry: the *w/a*-ratio at cross section 1 is 0.369 and 0.395 respectively 0.402 for the others to meet 50 Ω, see Figure 7. The variation of the *w/a*-ratio along the cell direction is small. Therefore, a linear fitting function is chosen and fitted through the cross sections. The linear fit simplifies septum manufacturing as in equation (13).

$$\frac{w}{a}(l) = \frac{0.000028}{mm} \cdot l(mm) + 0.3662 \qquad l = [100\,mm \ldots 1312\,mm] \tag{13}$$

The absolute septum width *w(l)* is defined by the cell width a. To fulfil the requirement of sufficient testing volume, a is set to 68 mm at l = 100 mm. Hence, *w(l)* is defined as:

$$w(l) = 0.213 \cdot l(mm) + 3.8539\,mm \qquad l = [100\,mm \ldots 1312\,mm] \tag{14}$$

Figure 8 shows the resulting *w/a*-ratio in the range from 100 mm to 1312 mm and the resulting wave impedance whose error e < 0.1 Ω is considered tolerable.

3.5 APEX GEOMETRY

The apex has to be determined separately because its *h/d*-ratio cannot be kept constant: the connector to the external attached coaxial cable demands an inner conductor with a *h/d*-ratio = 1/2 (centric). Hence, the first 100 mm of the septum have to adjust the *h/d*-ratio to 3/4 by keeping the 50 Ω condition. The height adjustment is chosen linear over the apex's length for simplified manufacturing. Additionally, the septum thickness u significantly influences the wave

impedance due to the small absolute height d of the cell in this area. The resulting apex shape needs to address all three issues. Therefore, a FEM simulation for 5 equidistant cross sections is performed to create an apex geometry meeting $Z = 50\ \Omega$.The cross section at $l = 100$ mm is optimized to meet the septum geometry at h/d-ratio = 3/4. The result is fitted using a forth order polynomial. Equation (15) defines the apex width w_a along the cell's length l. Figure 8 shows the corresponding w/a-ratio of the apex and the resulting wave impedance in the range from 0 mm to 100 mm.

$$w_a(l) = -\frac{1.79 * 10^{-8}}{mm^3} * l^4 - \frac{4.934 * 10^{-6}}{mm^2} * l^3 - \frac{2.048 * 10^{-4}}{mm} * l^2 + 0.276 * l + 6.309\text{mm} \qquad (15)$$
$$l = [0\ mm \ldots 100\ mm]$$

3.6 WAVE IMPEDANCE OF THE GTEM CELL

The overall resulting wave impedance along the cell's geometry is shown in Figure 8.

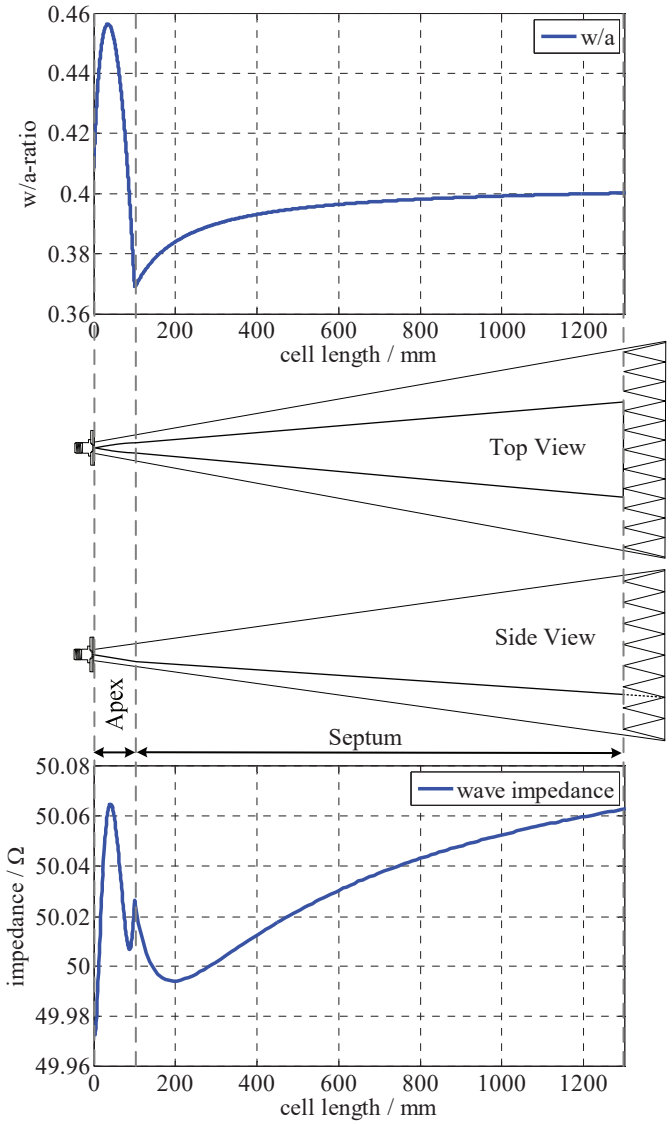

Figure 8. w/a ratio and resulting calculated impedance defined by apex and septum along cell length.

From 0 to 100 mm, the apex geometry is used to compensate the influence of the apex thickness u and the adoption of the height ratio between cable connector and septum. The continuous, non-differentiable interconnection between apex and septum geometry is at 100 m. The absolute maximum deviation is 0.06 Ω or 2‰ of the septum's calculated wave impedance Z. Manufacturing tolerances are likely to exceed the calculated deviation.

3.7 TERMINATION

The galvanic termination of the septum has to be 50 Ω in order to avoid reflections. A planar resistance over the whole septum width is used. It consists of small, surface mounted resistors connected in parallel on a printed circuit board. These resistances provide small series inductivities and small stray conductivities. The distance between resistors has to be smaller than λ/10 of the minimum wave length at maximum frequency (1 mm for 3 GHz in oil) to avoid reflections. In addition, the field energy of the electromagnetic waves needs to be considered. Oil-stable EM absorbers and ferrite plates are attached on the cell's termination wall for attenuating EM waves in the GHz range, see Figure 9.

The cell is built meeting all discussed demands concerning wave impedance and termination. The final cell is shown in Figure 10. A changeable adaption flange suited for different sensor types is mounted on its top.

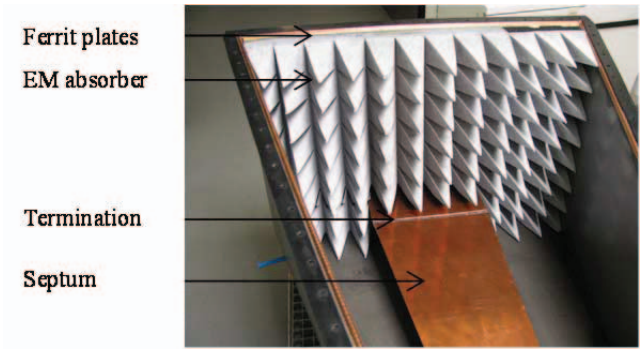

Figure 9. Oil-filled GTEM cell (interior view) [16].

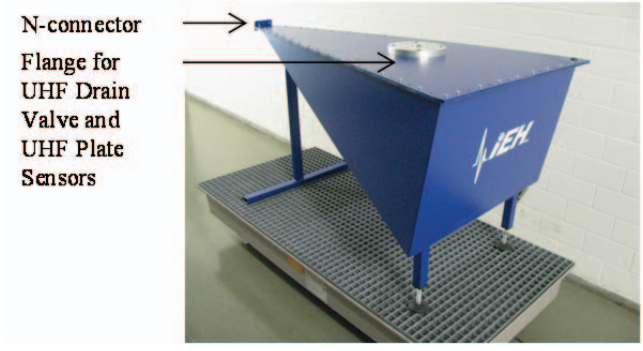

Figure 10. Oil-filled GTEM cell [16].

4 CELL EVALUATION

4.1 STANDING WAVE RATIO

Reflections at the end of the cell can lead to undesirable standing waves which impact one of the cell's major quality

factors: an inhomogeneous electric field distribution [19]. Standing waves are mainly influenced by the frequency depending cell termination which consist of the distributed resistors on the septum, the rear absorbers and ferrite plates. The voltage standing wave ratio SWR is defined by

$$SWR(f) = \frac{1 + |S_{11}(f)|}{1 - |S_{11}(f)|} \tag{16}$$

S_{11} is the reflection scattering parameter of the cell input port 1, compare Figure 4. The ideal cell provides a standing wave ratio of SWR = 1, meaning that the reflection is zero. Figure 11 shows the measured SWR of the constructed cell. The SWR from low frequencies to approx. 100 MHz depends on the resistance termination. The rising SWR up to 20 MHz is caused by the rising termination impedance due to the resistors' parasitic serial inductivity. In the range from 20 MHz to 100 MHz, the SWR is reduced by the superimposed effect of the resistors' serial stray capacity. The absorbers operate at frequencies above 400 MHz. Additionally, the ferrite plates are used in the intermediate frequency range. The resulting highest and therefore worst SWR of 1.724 occurs at 330 MHz. A conventional air-filled GTEM cell provides slightly lower values with $SWR_{max} \approx 1.5$ [20]. As a result, the cell quality is considered sufficient.

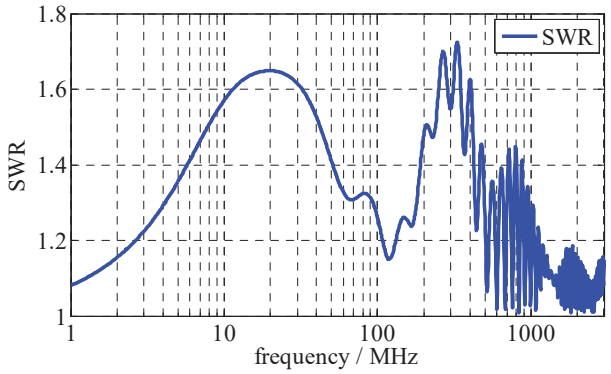

Figure 11. Measured SWR of the constructed oil-filled GTEM cell

4.2 TIME DOMAIN REFLECTOMETRY

The wave impedance along the cell's length is determined by time domain reflectometry (TDR). Aberrations from 50 Ω due to non-matched intersections or erroneous apex and septum geometries can occur. They can be detected by their reflectance factors in time domain. The test pulse is injected into the cell's input port and reflections are recorded. Ideally, the test pulse is a step function with infinite gradient. The real pulse provides a rise time of approx. 400 ps, which allows an evaluation of frequencies up to ~2 GHz. The measured reflection is shown in Figure 12. Signals are recorded using a digital storage oscilloscope (DSO) with 4 GHz analogue bandwidth and 40 GS/s sample rate.

The signal decrease at approx. t = 0.197 µs is caused by the transition from the 50 Ω cable to the cell at its input port. The reflection factor r can be calculated using equation (17), where the measured voltage $v_{measured}(t)$ is given by the superimposition of the propagating wave of the step function $f_h(t)$ and its reflection $r \cdot f_h(t)$. Using equation (18), the cell's wave impedance Z_{cell} can be derived from the reflection factor with the known cable wave impedance $\Gamma_{cable} = 50\ \Omega$.

$$v_{measured}(t) = f_h(t) + r f_h(t) \tag{17}$$

$$r = \frac{|Z_{cell}| - \Gamma_{cable}}{|Z_{cell}| + \Gamma_{cable}} \tag{18}$$

The reflection factor is determined to $r = -7.7 \cdot 10^{-3}$ and the resulting impedance is $Z_{cell} = 49.2\ \Omega$. The small error of 1.6% is tolerable. The voltage signal remains reduced for approx. $t = 13$ ns, which is the time the signal needs to travel forward and backwards after it is reflected at the non-ideal termination. The phase velocity is $v_{phase} \approx 2/3\ c_0$ in oil due to $\varepsilon_r = 2.2$, see equation (10). The local maximum and the successive exponential signal decrease at the end are caused by the combination of the termination resistors and their parasitic inductivity, see chapter 4.1. The combination of a tolerable SWR and the well wave impedance of the cell measured by TDR qualify the GTEM cell as reference test setup for UHF sensor's AF estimation.

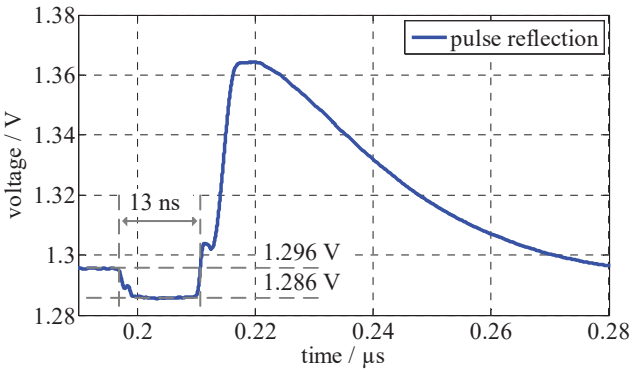

Figure 12. Result of TDR measurement on oil-filled GTEM cell.

5 ANTENNA FACTOR MEASUREMENTS

The AFs of UHF Drain Valve and UHF Plate Sensors are evaluated with the cell. Sensors are inserted through the cover plate of the cell into the testing volume. The antenna is aligned along the vertically orientated electric field which avoids polarisation losses during measurement. The whole antenna must be within the testing volume of the cell which provides the homogenous field of the TEM wave. The cell is excited with constant signal power $P_{sig} = 10$ dBm on its input port 1 using a VNA. Frequencies are considered from 300 kHz to 3 GHz. The resulting electric field E at the antenna position can be estimated using equation (19), where h is the distance between the septum and the cell's cover plate.

$$E = \frac{U_1}{h} = \frac{\sqrt{P_{sig} \cdot Z_{cell}}}{h} \tag{19}$$

The equation is only accurate for two infinite conducting plates. The real electrostatic field distribution can be simulated using a 2D model of the cell's cross section at the antenna position. The simulation includes the field attenuations caused by the gate valve (different boundary conditions). The theoretical results can be evaluated by electric field probe measurements. Unfortunately, oil-resistant probes in cell-

suited dimensions were not available during the first evaluation of the cell. A field evaluation based on measurements will be included in future works.

Figure 13 shows the UHF Drain Valve Sensor configurations with and without gate valve and a wall-mounted UHF Plate Sensor. The gate valve influences the sensor's ground plane geometry and has to be considered separately.

The UHF Drain Valve Sensor is tested with the following positions:

- Pos. 1: The antenna is still inside the gate valve which is an undesirable installation but does occur at practical measurements.
- Pos. 2 is the most common case for transformer installations. The antenna just reaches into the transformer's tank volume.
- Pos. 3-5. These insertion depths are often not possible as sufficient distance to the HV windings must be maintained to ensure save insulation.

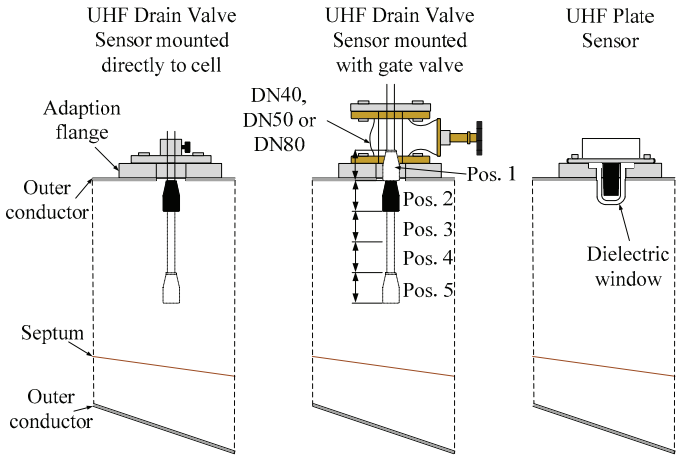

Figure 13. UHF Sensors mounted to the GTEM cell: UHF Drain Valve Sensor mounted directly, UHF Drain Valve Sensor mounted with gate valve and UHF Plate Sensor with dielectric window.

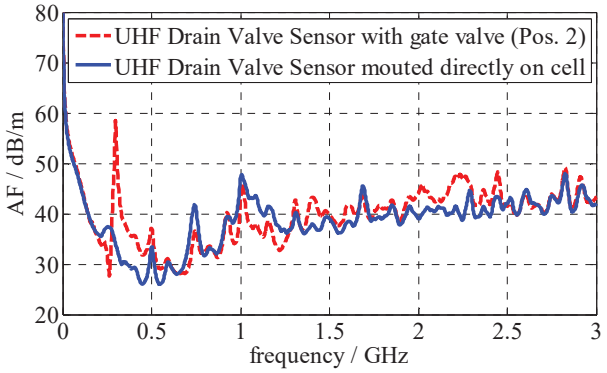

Figure 14. Influence of gate valve on AF of UHF Drain Valve Sensor measured in GTEM cell.

A small AF represents a sensitive antenna, see equation (1). The determined UHF Drain Valve Sensor is most sensitive from 200 MHz to 1 GHz with AF < 40 dB/m, see sensor without gate valve in Figure 14 (blue curve). For higher frequencies, the AF slowly increases from approximately 40 dB/m to 45 dB/m. The gate valve's main influence is a local maximum of the AF at 300 MHz. Figure 15 illustrates the influence of different insertion depths of an UHF Drain Valve sensor with gate valve.

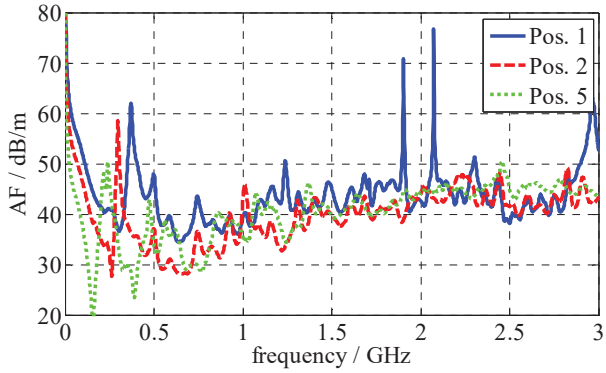

Figure 15. Influence of insertion depth on AF of UHF Drain Valve Sensor measured in GTEM cell with gate valve.

Best AFs are achieved at high insertion depth, see Pos. 5, but improvements are small at frequencies $f > 1$ GHz. The local maximum caused by the gate valve is shifted to lower frequencies. The worst case installation at Pos. 1 increases the AF especially at frequencies $f < 1$ GHz. Additionally, new peaks occur at 1.9 GHz / 2.1 GHz and at frequencies $f > 2.6$ GHz. Hence, this position is not desired for any UHF PD measurement.

Figure 16 compares the UHF Drain Valve Sensor in a gate valve at Pos. 2 with the UHF Plate Sensor. Both insertion depths are similar, but the Plate Sensor is not influenced by a valve. Therefore, the local maximum at 300 MHz does not exist. Both sensors are comparable in the frequency range $f = 500$ MHz…1.6 GHz. At higher frequencies, the UHF Drain Valve Sensor is slightly more sensitive due to two local maxima of the UHF Plate Sensor at 1.7 GHz and 2.6 GHz. In a general comparison, both sensor types are suited for transformer application. The Plate Sensor is considered slightly advantageous because of its smaller AF in the usually used frequency range $f < 1$ GHz.

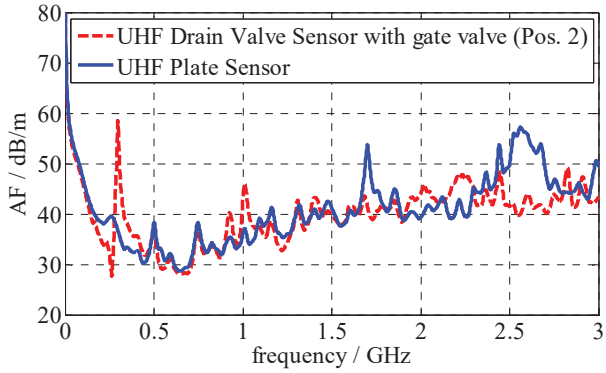

Figure 16. Comparison of UHF Plate Sensor and UHF Drain Valve Sensor.

6 CONCLUSION

The UHF method requires a calibration process, similar to the calibration of the electrical measurement (IEC 60270). Otherwise, measurements of different systems cannot be compared, which is a basic requirement for an accepted PD test method. In contrast to the electrical measurement, it is not possible to calibrate the entire UHF measurement path as the UHF sensor is excluded from the calibration path between calibrator and PD recording unit. Therefore, the sensor's characteristics have to be obtained separately and then included into the system calibration. A standard setup like the presented GTEM cell provides sensor characteristics by measuring the antenna factor. The introduced custom-made oil-filled GTEM cell covers the UHF frequency range from $f = 300$ MHz…3 GHz in 50 Ω domain and offers a known electric field strength in the testing volume. Its electrical properties are evaluated by standing wave ratio and time domain reflectometry measurements.

The cell is compatible to various mounting systems. Exemplary, two different UHF sensor types are characterized and compared: an UHF Drain Valve Sensor and an UHF Plate Sensor which can be integrated directly into transformer tank walls using a dielectric window. The determination of different UHF Drain Valve Sensor insertion depths reveals little influence on the sensor's sensitivity whereas the used gate valve itself leads to higher antenna factors and reduced sensitivity at frequencies in the lower 100 MHz range. Generally, the determined UHF sensors are most sensitive in the range from 200 MHz to 1 GHz.

The obtained antenna factors can be used to include the sensors into the calibrated path. Thus, the entire measurement path becomes calibrated and UHF measurements can become comparable independent of the used UHF sensors, cables or UHF measurement recorders.

REFERENCES

[1] International Electrotechnical Commission (IEC), "IEC 60270 High Voltage Test Techniques - Partial Discharge Measurements," Geneva, Switzerland, 2000.

[2] CIGRE TF 15/33.03.05, "PD Detection Systems for GIS: Sensitivity Verification for the UHF Method and the Acoustic Method," *International Council on Large Electric Systems, Electra No. 183,* 1999.

[3] S. Meijer, E. Gulski, J. Smit and H. Reijnders, "Sensitivity Check of UHF PD Detection on Power Transformers," *IEEE* IEEE Int0'l. Sympos. Electr. Insul., pp. 58-61, 2004.

[4] A. Reid, M. Judd, R. Fouracre, B. Stewart and D. Hepburn, "Simultaneous Measurement of Partial Discharges using IEC60270 and Radio-frequency Techniques," IEEE Trans. Dielectr. Electr. Insul., Vol. 18 , No. 2, pp. 444-455, 2011.

[5] S. Coenen, A. Müller, M. Beltle and S. Kornhuber, "UHF and acoustic Partial Discharge Localisation in Power Transformers," Paper No. D-015, Int'l. Sympos. High Voltage Eng. (ISH*)*, Hannover, Germany, 2011.

[6] CIGRE WG D 1.33, Guidelines for Unconventional Partial Discharge Measurements, Int'l. Council on Large Electric Systems, Paris, France, 2010.

[7] M. Judd, "Partial Discharge Monitoring for Power Transformers Using UHF Sensors Part 1: Sensors and Signal Interpretation," IEEE Electr. Insul. Mag., Vol. 21, No. 2, pp. 5-14, 2005.

[8] S. Tenbohlen, M. Siegel, M. Beltle and M. Reuter, "Suitability of Ultra High Frequency Partial Discharge Measurement for Quality Assurance and Testing of Power Transformers", CIGRE SC A2 & C4 Joint Colloquium, Zürich, Switzerland, 2013.

[9] A. Pfeffer, S. Tenbohlen and S. Kornhuber, "Influence of PD Location and Frequency Ranges on measured Apparent Charges," Paper No. D-040, Int'l. Sympos. High Voltage Eng. (ISH), Hannover, Germany, 2011.

[10] S. Okabe, G. Ueta and H. Wada, "Partial discharge signal propagation characteristics inside the winding of gas-filled power transformer - study using the equivalent circuit of the winding model," IEEE Trans. Dielectr. Electr. Insul., Vol. 18, No.5, pp. 1668-1677, 2011.

[11] S. Coenen, S. Tenbohlen, T. Strehl and S. Markalous, "Fundamental Characteristics Of UHF PD Probes And The Radiation Behavior Of PD Sources In Power Transformers," Paper No. C-26, Int'l. Sympos. High Voltage Eng. (ISH*)*, Cape Town, South Afrika, 2009.

[12] M. Judd and O. Farish, "A Pulsed GTEM System for UHF Sensor Calibration," IEEE Trans. Instrumentation and Measurement, Vol. 47, No. 4, pp. 875-880, 1998.

[13] International Electrotechnical Commission (IEC), "IEC 61000-4-20 ed2.0 Electromagnetic compatibility (EMC) - Part 4-20: Testing and measurement techniques - Emission and immunity testing in transverse electromagnetic (TEM) waveguides," IEC, 2010.

[14] C. Paul, *Introduction to Electromagnetic Compatibility,* New Jersey, USA: John Wiley & Sons, 2006, p. 202.

[15] D. Pozar, *Microwave Engineering,* New Jersey, USA: John Wiley & Sons, 2005.

[16] M. Siegel and S. Tenbohlen, "Design of an Oil-filled GTEM Cell for the Characterization of UHF PD Sensors," Paper No. PB-31, Int'l. Conf. Condition Monitoring and Diagnosis (CMD*)*, Jeju, Korea, 2014.

[17] E. Yamashita and K. Atsuki, "Strip line with rectangular outer conductor and three dielectric layers," IEEE Trans. Microwave Theory and Techniques, Vol. 18, No. 5*,* pp. 238-244, 1970.

[18] P. Tipler, *Modern Physics*, 4th edition, Palgrave Macmillan, 2003.

[19] C. Icheln, P. Vainikainen and P. Haapala, "Application of a GTEM cell to small antenna measurements," IEEE Int'l. Sympos. Antennas and Propagation Society, Montreal, Canada, pp. 546-549, 1997.

[20] ETS Lindgren, *Model 5400 Series Gigahertz Transverse Electromagnetic* (*GTEM!™*), Cell Operation Manual,“ 2014.

Martin Siegel received his Dipl.-Ing. degree in electrical engineering from the University of Stuttgart, Stuttgart, Germany, in 2010. His diploma thesis was about the integration of electric vehicles in a grid with a high proportion of renewable energies. Since 2011, he is an academic researcher at the Institute of Power Transmission and High Voltage Technology, University of Stuttgart, where he operates in the field of power transformer diagnostics and monitoring. His current research interests include the applicability of unconventional partial discharge measurement methods for online monitoring and localization at power transformers. Mr. Siegel is a member of CIGRE and the German Power Engineering Society VDE-ETG.

Michael Beltle received his Dipl.-Ing. degree in electrical engineering from the University of Stuttgart, Germany, in 2009. In his diploma thesis he was involved in determining degrading effects of electrostatic discharges on microcontrollers in automotive applications. He has been an academic researcher at the Institute of Power Transmission and High Voltage Technology, University of Stuttgart, where he is involved in the field of power transformer diagnostics and determines the long-term development of partial discharges and investigates the mechanical vibrations of active parts of transformers. He is a member of CIGRE and the German Power Engineering Society VDE-ETG.

Stefan Tenbohlen (M'04-SM'14) received his Diploma and Dr.-Ing. degrees from the Technical University of Aachen, Germany, in 1992 and 1997, respectively. In 1997 he joined ALSTOM Schorch Transformatoren GmbH, Mönchengladbach, Germany, where he was responsible for basic research and product development. From 2002 to 2004 he was the head of the electrical and mechanical design department. In 2004 he was appointed to a professorship and head of the institute of Power Transmission and High Voltage Technology of the University of Stuttgart, Germany. In this position his main research fields are high voltage technique, power transmission and electromagnetic compatibility (EMC). Prof. Tenbohlen holds several patents and published more than 300 papers. He is member of the IEEE, CIGRE SC A2 (Power Transformers), German committees of A2, D1 (Emerging Technologies), C4 (System Technical Performance), several international working groups and the chairman of German Power Engineering Society VDE-ETG FB Q2 (Materials, Electrical Insulations and Diagnostics).